Effect of energetic disorder on triplet-triplet annihilation in organic semiconductors

Mohammad Amir Bazrafshan, Mehdi Ansari-Rad,* and Saeid Hessami Pilehrood
Faculty of Physics, Shahrood University of Technology, Shahrood 3619995161, Iran

(Received 30 December 2019; revised manuscript received 1 March 2020; accepted 9 March 2020; published 24 March 2020)

We present a model for the triplet-triplet annihilation in organic phosphorescent host-guest systems that considers the effect of the energetic disorder on the kinetics of the annihilation. Nonequilibrium (time-dependent) transport of the triplets that arises from the progressive relaxation of triplets in the energy landscape is taken into account in the model. Triplet excitons are considered to move between the guest sites (dye molecules) via the thermally activated tunneling mechanism; the annihilation step, however, takes place through the Förster mechanism. Based on the model developed, and by calculating the time evolution of the triplet concentration, we investigate the effect of the various parameters on the effective annihilation coefficient. At low dye concentrations, it is shown that relaxation of the triplets is not completed during their lifetimes, and therefore, the annihilation process occurs entirely in the nonequilibrium. We also address the competition between two pathways for the annihilation process: single-step, long-range annihilation, and diffusion-assisted annihilation. By a quantitative comparison with experimental data reported in the literature, we demonstrate certain conditions in which there is a considerable contribution from the diffusion to the total annihilation rate. The model presented in this work can also be used for the excitons that diffuse by the Förster mechanism.

DOI: 10.1103/PhysRevB.101.094204

I. INTRODUCTION

Organic semiconductors and related molecular systems have attracted great attention in science and technology in recent decades owing to their (potential) applications in various electronic and optoelectronic devices [1,2]. A key factor determining the performance of these devices is how efficient energy excitations (singlet and/or triplet excitons) transfer between the structural units of the system. For example, the diffusion length of the excitons in organic photovoltaics plays a determining role in the charge separation efficiency of the photovoltaic cell [3]. In organic photon up-conversion systems, also, the up-conversion yield is determined by the triplet-triplet annihilation (TTA) process in which two triplets that are in the vicinity of each other annihilate, resulting in a delayed fluorescence [4,5]. The TTA in phosphorescent OLEDs, in contrast, leads to a loss in the population of the triplet excitons, resulting in the so-called efficiency roll off and a limited brightness at high triplet densities [6,7]. In these devices, as a consequence of the radiative decay of the triplet excitons, the phosphorescent light is emitted by guest dye molecules dispersed in an organic host system. An efficient diffusion of the triplet excitons between the dye molecules, however, brings the triplets to the neighborhood of each other and enhances the rate of the TTA consequently. This picture, which highlights the role of the diffusion [8–12], however, has been under debate in the literature [13–16]: it has been concluded in some research that it is mainly the direct (single-step) annihilation process that governs the photoluminescence (PL) kinetics of the system and the effect of the diffusion is marginal. Therefore, deciding what strategies are needed to be developed to prevent the efficiency roll off in phosphorescent OLEDs (or, to boost the up-conversion yield in photon up-conversion systems) relies on the detailed understanding of the effect of the triplet diffusion on the TTA rate. In this paper, we discuss how and to what extent the triplet diffusion influences the annihilation process in the typical host-guest emitting systems.

One of the general features of the organic and molecular systems is that, because of the inherent structural and orientational disorder in the system, there is not a sharp, well-defined LUMO energy state (T_1 energy state) for the excitons; instead, one deals with a distribution of localized states, which makes the system energetically disordered. It is believed that the transport of the spatially localized excitons (the so-called Frenkel excitons) occurs via the incoherent hopping of the excitons between the neighboring sites; here, between the dye molecules [17,18]. One can quantify this hopping transport with a diffusion coefficient, although because of the disorder, this coefficient can show a complex dependency on the temperature of the system, the strength of the disorder, and the dye concentration, as discussed elsewhere [19,20]. In this work, however, we are going to address the nonequilibrium feature of the transport process, also known as dispersive transport, which arises because of the progressive relaxation of the excitons in the energy landscape. Although the nonequilibrium transport of exciton and its effect on the TTA has been studied using the kinetic Monte Carlo (kMC) simulations [21], following our recent work on the description of the singlet transport [22], here we present a theoretical model that can describe both the nonequilibrium (dispersive) and equilibrium transport of the triplet excitons. Using this time-dependent diffusion coefficient, then, the equation that

*ansari.rad@shahroodut.ac.ir

governs the temporal evolution of the triplet concentration is solved numerically. We also present a direct comparison with the kMC simulation results and the PL measurements recently reported for the TTA rate in the host-guest systems. In what follows, we first give our theoretical model regarding the TTA and triplet diffusion process in the energy disordered systems, Secs. II A and II B. The next section will be devoted to the results obtained in this work (Sec. III): we first present the results for the diffusion coefficient, and its dependency on the various parameters is discussed. In the following, then, our results for the TTA rate will be discussed in detail. Finally, Sec. IV gives the conclusion and summary.

II. THEORY AND MODELING

A. Annihilation rate coefficient

We consider the PL response of a system of dye molecules with concentration N, randomly dispersed in a host matrix, to a pulse illumination. Upon the illumination, an initial population of triplet excitons with a total concentration of ρ_0 is generated on the dye molecules whose time evolution is given by

$$-\frac{d\rho}{dt} = \frac{\rho}{\tau} + \frac{1}{2}k_{\mathrm{TT}}(t)\rho^2. \tag{1}$$

Here τ is the unimolecular triplet lifetime and $k_{\mathrm{TT}}(t)$ is the TTA rate coefficient. The factor $1/2$ in Eq. (1) accounts for the fact that usually only one triplet is assumed to be lost in a TTA event, that is, $T + T \rightarrow S_0 + T$ where T and S_0 stand for the triplet excitation and an unexcited molecule, respectively. Note that experimentally both N and ρ_0 can be controlled and tuned with sufficient precision.

Equation (1) is itself originated from the continuity equation that governs the local concentration of the triplets. Therefore, three factors determine the functional form of the rate coefficient $k_{\mathrm{TT}}(t)$. The first is the so-called inner boundary conditions (BCs) of the continuity equation, which describes the annihilation process when two triplets reach a close vicinity of each other. Two possible BCs are the Smoluchowski and the partially absorbing BC. For future reference, one notes that in the Smoluchowski BC there is an encounter distance R_c at (or, below), which the annihilation process between two triplets occurs with probability one. The second is the fundamental rate by which a TTA event occurs. For two triplets that are at distance R from each other, this rate is assumed to be given by the Förster expression

$$\nu_{\mathrm{F}}(R) = \frac{1}{\tau_{\mathrm{F}}}\left(\frac{R_{\mathrm{F}}}{R}\right)^6, \tag{2}$$

with $\tau_{\mathrm{F}} = \tau/2$ and R_{F} being the lifetime and Förster radius for the TTA, respectively. According to the Förster theory, the radius R_{F} is determined by the spectral overlap of the triplets participating in the annihilation process. Also, since the origin of the Förster process is the dipole-dipole interaction between the dye molecules, R_{F} also depends on the orientation of those dipoles [23,24]. Assuming that the dipoles are free to rotate with a rate that is much higher than the transport or annihilation rate [23,25], the radius R_{F} can be considered to be the same in each annihilation event. On the opposite limit of the fixed orientations also, one can interpret R_{F} as an average value over all possible annihilation processes [12]. As a consequence, in the following, we consider the Förster radius as a constant parameter in our considerations.

The third factor, finally, is the diffusive motion of the triplet excitons (with the diffusion coefficient D), which brings them towards each other and thereby accelerates the annihilation process. The diffusive motion comes from an incoherent transfer of triplet excitons among the dye molecules that for excitons that purely have triplet character, is given by the Dexter expression [17],

$$\nu_{\mathrm{diff}}(R) = \nu_0 \exp\left(-2\frac{R}{\alpha}\right). \tag{3}$$

Here ν_0 is the attempt-to-jump frequency, α is a measure of the spatial extent of the exciton wave function, and R is the jump distance between the donor and the acceptor dye molecule. Note that our choice for describing the TTA as a Förster transfer and, on the other hand, triplet diffusion motion as a Dexter transfer has been based on the quantum-mechanical selection rules [23]. Experimental evidence also supports Förster-type TTA in phosphorescent emitters [14,26] and Dexter-type triplet diffusion in organic semiconductors [27]. (Triplet diffusion in Ref. [16], however, has been described as a Förster transfer since it was assumed that, because of the spin-orbit coupling, the spin of the exciton need not be conserved during the transfer process and therefore the above-mentioned selection rule does not apply for the triplet.) In the following, we also assume that the T_1 energy difference between the host and dye molecules is high enough to assure complete confinement of the triplet excitons in the dye molecules. Therefore, in the following, we neglect the possibility of host-mediated diffusion in our modeling. This assumption is reasonable since energy differences of the order of 0.2–0.5 eV are quite common in state-of-the-art phosphorescent OLEDs, which has been concluded to be adequate to establish strong confinement [28]. As we discuss in detail below, for the excitons that hop according to Eq. (3) we have $D = D(t, \nu_0, \alpha, N, \sigma/k_{\mathrm{B}}T, \rho_0)$, where σ is the variance of the energy disorder that may exist in the system and $k_{\mathrm{B}}T$ is the thermal energy. We also show that even for disorder-free transport, i.e., for $\sigma/k_{\mathrm{B}}T \ll 1$, the diffusion coefficient exhibits time dependence during the exciton lifetime, especially at small N [29] in which this time dependency can extend over the exciton lifetime.

Considering the Smoluchowski BC for the excitons that annihilate according to the Förster rate and diffuse with the diffusion coefficient D, Gösele *et al.* suggested that the rate coefficient $k_{\mathrm{TT}}(t)$ can be expressed as [30]

$$k_{\mathrm{TT}}(t) = 8\pi R_{\mathrm{eff}} D\left[1 + \frac{R_{\mathrm{eff}}}{\sqrt{2\pi t D}}\right] \tag{4}$$

with

$$R_{\mathrm{eff}} = A_z\left(\frac{R_{\mathrm{F}}^6}{D\tau_{\mathrm{F}}}\right)^{\frac{1}{4}}. \tag{5}$$

Although there is not a general consensus about the coefficient A_z (especially in the case $D \rightarrow 0$), Butler and Pilling [31] and then Rice [32] have discussed in detail that the following expression gives excellent agreement with the numerical

solution of the continuity equations in almost all cases:

$$A_z = \frac{\Gamma\left(\frac{3}{4}\right)}{2\Gamma\left(\frac{5}{4}\right)}\left[1 + \frac{\sqrt{2}}{\pi}\frac{K_{1/4}(z)}{I_{1/4}(z)}\right], \tag{6}$$

where $z = (R_F^6/4R_c^4 D\tau_F)^{\frac{1}{2}}$, and $I_{1/4}$ and $K_{1/4}$ are the modified Bessel functions of the first and second kind, respectively. Here, however, we must point out that since in realistic situations the rate ν_F always remains finite in comparison with ν_{diff}, the Smoluchowski condition is not likely to be fulfilled in the experiments. Also, we note that the role of the diffusion is merely to redistribute the excitons among the dye molecules and the final stage of a TTA event, even at $R \leqslant R_c$, should be determined only by the rate ν_F. Therefore there should not be an unphysical distance R_c in the formulation, which introduces an extra pathway for the annihilation process in addition to the Förster transfer. Consequently, we suggest to use Eq. (6) with $R_c \to 0$ (i.e., $z \to \infty$) that results in the following constant for the coefficient in Eq. (5)

$$A_{z\to\infty} = \frac{\Gamma\left(\frac{3}{4}\right)}{2\Gamma\left(\frac{5}{4}\right)} \approx 0.676. \tag{7}$$

In the following, for brevity, we use the symbol A for $A_{z\to\infty}$. It should be noted that setting $R_c \to 0$ does not imply that two excitons are allowed to occupy a single dye molecule simultaneously. Instead, this is the dye concentration that determines the shortest possible distance between two excitons, which is roughly given by $1/N^{\frac{1}{3}}$. As we show in the next section, this requirement is automatically satisfied in our modeling when we calculate the diffusion coefficient.

With $k_{TT}(t)$ in hand, one can integrate Eq. (1) to obtain $\rho(t)$. By fitting the $\rho(t)$ to simulation or experimental PL results then, one can find $k_{TT}(t)$ that best fits the data. It has been found, however, that due to noise of the PL data and the sensitivity of the fit to the noise, especially at long times or small ρ_0, this method may yield a large error. Also, since $k_{TT}(t)$ is time dependent, it is worthwhile to introduce an effective rate coefficient k'_{TT} to quantify the annihilation process with a single number [note that besides its explicit time dependence seen in Eq. (4), we may have $D = D(t)$ as we show below]. Recently, Eersel *et al.* [11] have proposed using the relative cumulative PL as a method to suppress the noise and give a definition for k'_{TT}. A detailed explanation of how this method is practically applied for the experimental data can be found in Refs. [15,28]. According to this method, we first compute the relative cumulative PL from $\rho(t)$ as

$$\eta^{rel}_{cum,PL}(t) = \frac{1}{\tau}\int_0^t \frac{\rho(t')}{\rho_0}dt'. \tag{8}$$

The saturated relative cumulative PL, $\eta^{rel}_{cum,PL}(t = \infty)$, is then equated to the value that one would obtain if one used Eq. (1) with a time-independent rate coefficient k'_{TT}, i.e.,

$$\eta^{rel}_{cum,PL}(\infty) \equiv \frac{2\ln(1 + \rho_0\tau k'_{TT}/2)}{\rho_0\tau k'_{TT}}. \tag{9}$$

In Fig. 1 we present a flowchart showing the numerical procedure we use in this work to compute k'_{TT}. Steps needed to compute the diffusion coefficient are also illustrated in the figure, which will be discussed in detail in the following section.

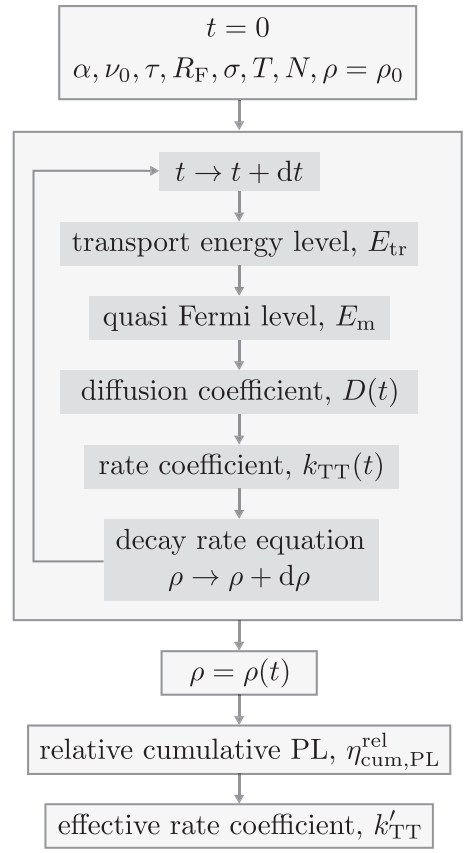

FIG. 1. Schematic flowchart of the computational steps applied for calculating the effective TTA rate coefficient. See main text for further details.

B. Transport coefficient

As pointed out in Sec. I, due to the inhomogeneity in the local environment experienced by different dye molecules, there is a distribution of T_1 energy states of the excitons in the system. This energy distribution, denoted below by $g(E)$, is assumed to be Gaussian with a total density of N (equal to the dye concentration) and with a variance of $\sigma \simeq 2$–$3\,k_BT$. Therefore, the hopping of the excitons among the dye molecules is, in fact, a phonon-assisted process, and the Dexter jump rate given by Eq. (3) should be corrected by a temperature-dependent multiplying factor. Considering hopping of an exciton between two sites (dyes) i and j, this factor should satisfy the detailed-balance condition

$$\frac{\nu^{i\to j}_{diff}}{\nu^{j\to i}_{diff}} = \exp\left(-\frac{E_j - E_i}{k_BT}\right). \tag{10}$$

We note that besides the energetic disorder (here quantified by the variance σ), polaronic effects, i.e., environment polarization when a triplet resides in a dye molecule (quantified by a reorganization energy) may also play a role in the exciton transport. However, as noted in Ref. [18], in systems with the high energetic disorder the effect of the disorder becomes dominant and the polaronic effect can be neglected. In this

situation, the simplest transfer rate that satisfies Eq. (10) is the Miller-Abrahams rate, which is given by [33]

$$\nu_{\text{diff}}^{i\to j}(R) = \nu_0 \exp\left(-2\frac{R}{\alpha}\right) \times \begin{cases} \exp\left(-\frac{E_j - E_i}{k_B T}\right) & (E_i < E_j) \\ 1 & (E_i > E_j) \end{cases}. \tag{11}$$

In this work, we consider the Miller-Abrahams rate in our modeling. However, it should be noted that there is experimental evidence suggesting that the polaronic effects cannot be neglected when describing the triplet diffusion at high temperatures [34,35]. In this case, the temperature dependence of the transfer rate should be described by Marcus theory, as

$$\nu_{\text{diff}}^{i\to j} \propto \sqrt{\frac{\pi}{\lambda\, k_B T}} \exp\left(-\frac{\lambda}{4k_B T} - \frac{E_j - E_i}{2k_B T} - \frac{(E_j - E_i)^2}{4k_B T}\right) \tag{12}$$

in which λ is the reorganization energy [18]. Note that the Marcus rate also satisfies the detailed-balance condition. As suggested in Ref. [36], on the other hand, Miller-Abrahams theory can be more appropriate in describing the nonequilibrium diffusion.

Experimentally, it has turned out that in the energy disordered systems, excitons can be in the nonequilibrium phase during their whole lifetime [37–42]. For example, studying the PL spectrum of the organic semiconductors has revealed the so-called frustrated dynamics; a situation in which the triplet excitons vanish before their relaxation in the energy landscape is completed [36,40,43]. Very recently, we have shown how lowering the temperature slows down the relaxation process of the singlet excitons thereby preventing the excitons from reaching equilibrium [22]. One may note that any factor that suppresses hopping of the excitons among the dye molecules can delay the equilibrium regime. For example, considering Eq. (11), besides the temperature, a large average R (caused by a small dye concentration) or a small localization radius α can be determining factors in the relaxation process. As we see below, even in the absence of the disorder, a small N can result in a time-dependent diffusion coefficient. In conclusion, one notes that the equilibrium conditions (as assumed for example in Ref. [12]) may not necessarily be a valid assumption for the exciton dynamics during its lifetime. In Ref. [22] we presented a model based on the concept of the transport energy that can reproduce experimental data and kinetic Monte Carlo simulation results for the singlet excitons that diffuse according to the Förster mechanism. In the following, we adopt the same concept and apply the procedure for the triplet excitons, which transfer according to the rate presented in Eq. (11). We see that the model performs well in predicting the transport properties and annihilation features of the systems of interest.

Generally, there are two problems that make it difficult to study the exciton or charge transport in the energy disordered systems. The first is that, in contrast to the inorganic semiconductors, there is not a mobility edge in the energy landscape. Therefore the multiple-trapping picture (trapping into the localized states and subsequent detrapping to the mobility edge) seems not to be applicable here. Addressing this problem, it was shown that it is possible to define an energy level in the energy distribution, the so-called transport energy level E_{tr}, which plays the same role as the mobility edge in the multiple-trapping mechanism [20,44]. For excitons that transfer according to Miller-Abrahams rate, the transport energy is determined by solving the following transcendental equation [45] (see the following for the definition of the parameters; see also Supplemental Material [46])

$$\frac{2k_B T}{3\alpha}\phi(E_{\text{tr}}, E_f) = \left(\frac{4\pi}{3B_c}\right)^{\frac{1}{3}} \left[\int_{-\infty}^{E_{\text{tr}}} \phi(E, E_f)\, dE\right]^{\frac{4}{3}}. \tag{13}$$

In the above considerations, as in the previous studies on the TTA, we have assumed that the energy distribution in the system is spatially uncorrelated; the so-called Gaussian disorder model (GDM). However, it should be noted that because of, for example, long-range interactions between the electric dipole moments of the molecules, there may exist a spatial correlation between the dye energies, as first demonstrated for the charge transport in organic layers [47]. Although we do not consider this so-called correlated disorder model (CDM) in this work, using the master-equation method it has been suggested that the concept of transport energy for describing the transport according to the Miller-Abrahams rate is valid even for the CDM [48]. Therefore, by using an appropriate definition for computing the position of the transport energy level, our following calculations can, in principle, be applied for the case of the CDM also.

The second problem is that, due to the nonequilibrium conditions, one cannot define a Fermi level in the energy distribution and, consequently, statistical averaging methods [49,50] are not possible. By considering progressive relaxation of the electrons in an exponential energy distribution below a mobility edge, Tiedje and Rose defined a time-dependent energy level that separates electrons that during time t have experienced several multiple-trapping events, from those that have been immobilized in their initial sites [51]. Here, we adopt this picture but go a step further and interpret this energy as a time-dependent quasi-Fermi-level in the system, E_{m}. This enables us to perform statistical averaging to calculate the diffusion coefficient. As we have shown in Supplemental Material [46] one can finally obtain the following expressions for E_{m} and $D(t)$,

$$E_{\text{m}}(t) = E_{\text{tr}} - k_B T \ln(t\nu_0) + k_B T \left[\frac{\alpha^3 \pi k_B T}{18 B_c}\phi(E_{\text{tr}}, E_f)\right]^{-\frac{1}{4}} \tag{14}$$

and

$$D(t) = \frac{1}{t}\left(\frac{3B_c}{4\pi}\right)^{\frac{2}{3}} \frac{\left[\int_{-\infty}^{E_{\text{tr}}} \phi(E, E_{\text{m}})\, dE\right]^{\frac{1}{3}}}{\int_{-\infty}^{E_{\text{tr}}} \varphi(E, E_{\text{m}})\, dE}. \tag{15}$$

Here $\varphi = g(E) f(E, E_f)$ and $\phi = g(E)[1 - f(E, E_f)]$, where $f(E, E_f)$ is the Fermi distribution and E_f is the equilibrium Fermi energy determined by the population of the excitons, ρ. Note that all the energies are counted from the center of the Gaussian DOS $g(E)$, which is set to be zero. The constant factor $B_c = 2.735$ comes from the percolation theory, which demands that a mean number B_c of hopping sites with energy $\leqslant E_{\text{tr}}$ be available for upward hopping events [20,52]. Also, note that $D(t)$ of Eq. (15), as explained in Supplemental

Material [46], is an instantaneous diffusion coefficient. As it is illustrated in Fig. 1, the diffusion coefficient of Eq. (15) is finally fed into Eq. (4) to find $k_{TT}(t)$.

It should be noted that the above calculations rely on the assumption that the nonequilibrium relaxation can be described in terms of a system at equilibrium with time-varying parameters. Although a comparison with the previously reported kMC results, as we present in the following section, supports this assumption, it is useful here to provide a physical explanation for its validity. We first note that Eq. (1) is meaningful only if the differential dt is sufficiently smaller than the triplet lifetimes. On the other hand, since Eq. (1) describes the time evolution of a macroscopic parameter, ρ, dt should also be much larger than the microscopic time scale of the problem; ν_0^{-1}, for example. Besides the condition $\nu_0^{-1} \ll dt \ll \tau$, one also notes that Eq. (1) is valid if the change in the diffusion coefficient during time dt is negligible because, otherwise, $k_{TT}(t)$ is not definable in Eq. (1). Since the time dependence of the diffusion coefficient comes from the quasi-Fermi level E_m, the validity of the assumption of the quasistatic equilibrium is therefore determined by the time evolution of E_m. According to Eq. (14), at time t, change in the position of the quasi-Fermi level E_m during the time dt is $\Delta E_m = -k_B T\, dt/t$. Therefore, for the time scale relevant in the problem, τ, we obtain the condition $|\Delta E_m/k_B T| \ll 1$ for the validity of our assumption which is a plausible result showing that the quasi-Fermi level is a sufficiently slowly varying function of time.

Finally, before presenting our results in the next section, it is useful here to highlight the essential features of our modeling to make a comparison with the previous works in the field. We note that the dependence of $k_{TT}(t)$ on the energetic disorder, temperature, dye concentration, and triplet population comes from its dependency on the diffusion coefficient. In addition, because of the relaxation process, besides its apparent time dependence, $k_{TT}(t)$ can acquire additional dependency through the diffusion coefficient. Therefore, to study the TTA, it is important to provide a theoretical model that can describe the relaxation process, crossover to the equilibrium condition, and time dependency of the diffusion coefficient over a broad temperature range. Although elaborate numerical and theoretical models have been developed in the past decades in this field, to our knowledge, previous works on the TTA in disordered systems have been based on the existing transport theories, which are limited to the equilibrium condition, or based on the kMC simulations. (For a review on the transport in disordered systems, see Ref. [20]. Also, see, for examples, Refs. [11,12,16] for recent works on the annihilation process.) The model presented here, however, goes a step further and provides a tool to describe the effect of the energetic disorder, and the time dependency induced by the nonequilibrium transport, on the TTA process.

III. RESULTS AND DISCUSSION

Figure 2 shows the diffusion coefficient as a function of time, calculated using Eq. (15) for different dye concentrations and disorder parameters. We note that, in the systems of interest, typical phosphorescence lifetimes are of the order of $\tau = 1\,\mu$s. This characteristic time, therefore, can be considered as a criterion to determine whether D is constant or time dependent in the problem. We have indicated this timescale in the figure. As seen, at high concentration and weak disorder (upper curve), the diffusion coefficient is almost time independent, as expected. For strong disorder (0.065 eV, which is a typical value in organic semiconductors [25,40]) or lower dye concentration (10^{26} m^{-3}, which is relevant to OLEDs), however, the diffusion coefficient is time dependent. The origin of this time dependence is clear, as discussed elsewhere [49]: as time passes, because of the relaxation of the excitons in the energy landscape, their thermal activation to the transport energy level (that plays the role of the mobility edge) becomes more difficult, and consequently, D decreases with time. The relaxation process in a Gaussian DOS, however, stops when the average energy of the excitons reaches the equilibrium energy $-\sigma^2/k_B T$ [53], leading to a stationary value for the diffusion coefficient at long enough times. A similar argument holds for the effect of dye concentration on the diffusion process [29,54]. This effect is in fact in close similarity to the effect of porosity on the diffusivity in porous materials, where increasing the porosity extends the nonequilibrium regime and delays the stationary situation [55,56]. The results in Fig. 2 clearly show that at timescales relevant to the TTA, transport of the excitons may occur entirely in the nonequilibrium regime. This is in agreement with the earlier kMC simulation [21] and experimental results [57–59] that the kinetics of the annihilation in a disordered system can be governed by the dispersive diffusion of the excitons. Also, we note that the magnitude of the diffusion coefficient obtained for N' in Fig. 2 ($\sim 10^{-12}$ m$^2/s$) is consistent with the typical values observed for the triplet excitons in the disordered organic systems [8,27]. Since the diffusion coefficient is a time-varying quantity, in the following, when we present dependence of the diffusion coefficient on the various parameters, we only report $D_{t=\tau}$ (that is, the diffusion coefficient at the specific time $t = \tau$), which may or may not be the stationary value of the diffusion coefficient.

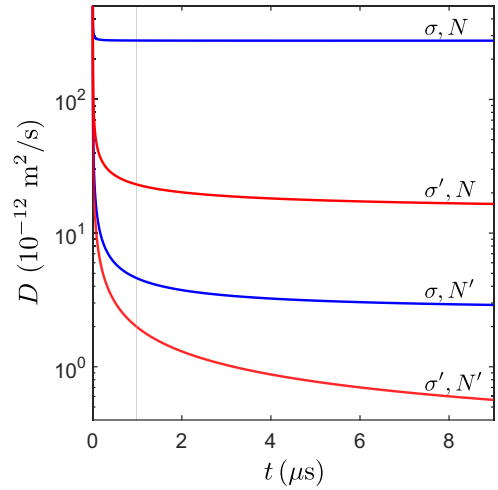

FIG. 2. Time evolution of the diffusion coefficient, as obtained from Eq. (15) for $T = 300$ K, $\alpha = 0.35$ nm, $\nu_0 = 5.5 \times 10^{11}$ s^{-1}, and $\rho_0 = 10^{24}$ m^{-3}. In the figure $\sigma = 0.025$ eV, $\sigma' = 0.065$ eV, $N = 10^{27}$ m^{-3}, and $N' = 10^{26}$ m^{-3}. The vertical line highlights the time $t = 1\,\mu$s, a typical lifetime of the triplet exciton.

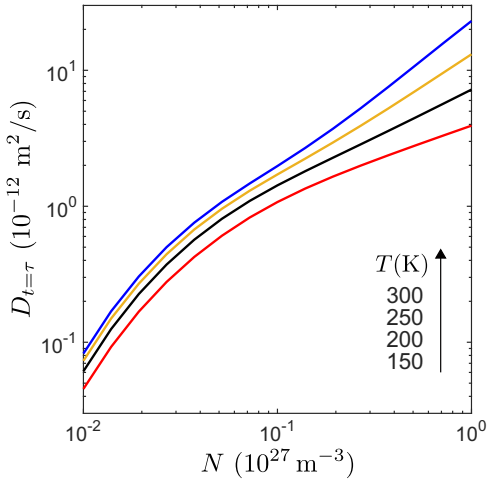

FIG. 3. Effect of the dye concentration on the diffusion coefficient at four different temperatures calculated from Eq. (15) with $\alpha = 0.35$ nm, $\nu_0 = 5.5 \times 10^{11}\ \mathrm{s}^{-1}$, $\rho_0 = 10^{24}\ \mathrm{m}^{-3}$, and $\sigma = 0.065$ eV. Since diffusion coefficient is time-dependent, its values at time $\tau = 1\ \mu$s have been plotted (see main text for details).

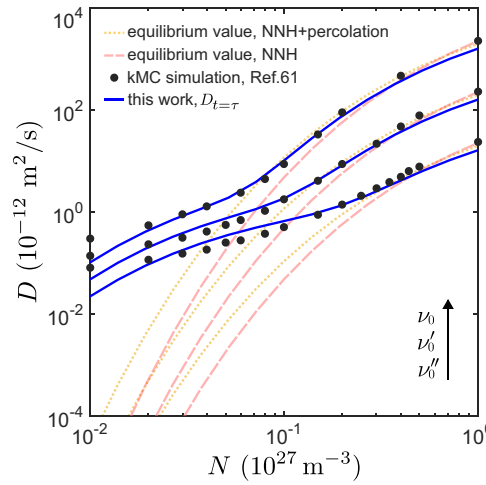

FIG. 4. The diffusion coefficient as a function of the dye concentration for a disorder-free system with $\alpha = 0.3$ nm, $\rho_0 = 10^{24}\ \mathrm{m}^{-3}$ and $\nu_0 = 1.6 \times 10^{12}$, $\nu_0' = 1.6 \times 10^{11}$ and $\nu_0'' = 1.6 \times 10^{10}\ \mathrm{s}^{-1}$. Solid curves: calculated using Eq. (15) at time $\tau = 1\ \mu$s. Filled circles: kMC simulation results from Ref. [61]. Dashed and dotted curves: prediction of Eq. (16) and Eq. (17), respectively (NNH stands for nearest neighbors hopping).

The dependence of the diffusion coefficient on the dye concentration is shown in Fig. 3 for four different temperatures, in a system with $\sigma = 0.065$ eV. As expected, $D_{t=\tau}$ monotonically increases with N, but as we see, the higher the temperature the stronger is the dependence of $D_{t=\tau}$ on N. This behavior can be understood by considering the Miller-Abrahams rate, and noting that there is an asymmetry between the temperature dependence of the upward and downward rates. At low concentrations, since the system is in the nonequilibrium regime, most of the jumps are downwards, which according to Eq. (11) are temperature independent. Therefore, the effect of the temperature on the diffusion coefficient is small. In contrast, at high concentrations, the system reaches the thermal equilibrium quickly (as we saw in Fig. 2), and in the equilibrium, the diffusivity is mainly determined by the upward jumps to the vicinity of the transport energy [60]. Consequently, the effect of the temperature on the diffusion coefficient increases with N. As discussed in the previous section, the Miller-Abrahams rate is not the only one that obeys the detailed-balance condition. Therefore, the explanation provided above appears to be specific to the choice of using the Miller-Abrahams rate. However, a similar argument can also be made for the other relevant rate expressions, which satisfy the detailed-balance condition. For example, if we consider the Marcus rate in Eq. (12), it can be seen that at the nonequilibrium regime, most probable downward jumps are the jumps with $E_j - E_i \approx -\lambda$, leading to $(E_j - E_i + \lambda)^2/4\lambda k_B T \approx 0$ irrespective of the temperature (note that this reasoning is correct if the energy difference between the sites can be as high as λ, or in other words, if $\lambda \leqslant \sigma$). Nevertheless, further work, especially the kMC simulation, will be necessary to validate our discussion.

Although the transport energy concept is generally believed to be valid only for $\sigma/k_B T > 1$, let us apply it to the case $\sigma/k_B T < 1$. Figure 4 shows the results of such calculations in the limiting case of $\sigma/k_B T \ll 1$, that is, for a system with (almost) no energetic disorder. To compare our results with the kMC simulation results reported in Ref. [61], the parameters in Fig. 4 were chosen from that reference. A very good agreement between the model (solid curves) and the kMC results (filled circles) is seen in the figure, implying that the method described here to calculate the diffusion coefficient is valid even for the case that $\sigma < k_B T$. In a system of randomly distributed dye molecules, the average distance between the hopping sites is $\ell = 1/N^{\frac{1}{3}}$. Therefore, in a disorder-free system, assuming a nearest-neighbor hopping (NNH) mechanism for the transport between the hopping sites, one can obtain the diffusion coefficient as

$$D_{\mathrm{NNH}} \approx \frac{\ell^2}{1/\nu_{\mathrm{diff}}(\ell)} = \frac{\nu_0}{N^{\frac{2}{3}}} \exp\left(-\frac{2}{\alpha N^{\frac{1}{3}}}\right). \tag{16}$$

In Fig. 4 we have also plotted the prediction of the above equation for the diffusion coefficient (dashed curves) that shows an agreement with the kMC simulation results only at high concentrations (strictly speaking, the region of the agreement is determined by $N\alpha^3$ and not merely by N). Based on the percolation theory together with the assumption of an NNH transport mechanism, however, a similar but not identical expression has been given for the diffusion coefficient, as [20,52]

$$D_{\mathrm{NNH,P}} \propto \frac{\nu_0}{N^{\frac{1}{3}}(\alpha N^{\frac{1}{3}})^{0.9}} \exp\left(-\frac{1.7351}{\alpha N^{\frac{1}{3}}}\right). \tag{17}$$

The dependence of the diffusion coefficient on the concentration of the dye molecules as predicted by Eq. (17) has been shown in Fig. 4 (dotted curves). As seen, in comparison with the ones predicted by Eq. (16), the agreement with the kMC simulations exists over a wider range of N. To explain the discrepancy observed in Fig. 4 between Eqs. (16) and (17) on one hand and the kMC simulation results on the other, it should be noted that both of the equations describe the equilibrium regime, whereas, as we saw in Fig. 2, at low concentrations

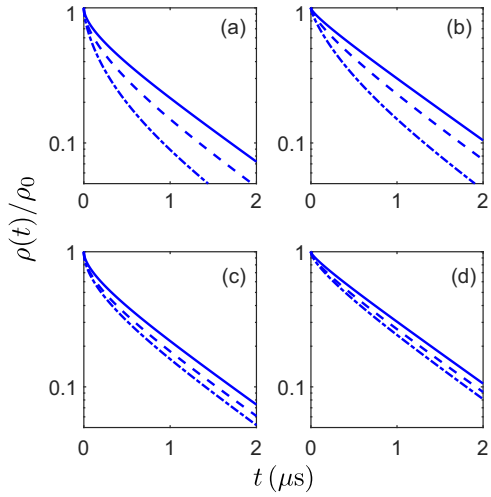

FIG. 5. Time evolution of the (normalized) triplet density for a system with $T = 300$ K, $\alpha = 0.35$ nm, $\nu_0 = 5.5 \times 10^{11}$ s^{-1}, $\rho_0 = 10^{24}$ m^{-3}, and $\tau = 1\,\mu$s. Solid curves, dashed curves, and dashed-dotted curves represent results for $N = 0.02$, 0.2, and 0.5×10^{27} m^{-3}, respectively. Also, top and bottom panels are for $\sigma = 0.025$ and 0.065 eV, respectively. (a), (c) $R_F = 5.5$ nm. b,d) $R_F = 3.5$ nm.

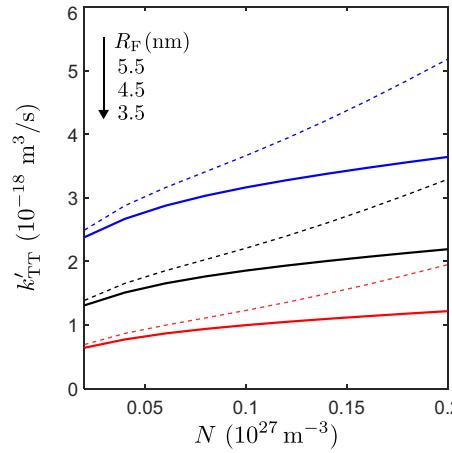

FIG. 6. Effective rate coefficient as a function of the dye concentration for three Förster radii and two different disorder parameters $\sigma = 0.025$ (dashed curves) and 0.065 eV (solid curves). Results are for $T = 300$ K, $\alpha = 0.35$ nm, $\nu_0 = 5.5 \times 10^{11}$ s^{-1}, $\rho_0 = 10^{24}$ m^{-3}, and $\tau = 1\,\mu$s.

the equilibrium assumption is not valid at times $t \sim \tau \sim 1\,\mu$s. As a conclusion to this discussion, our results suggest that the time dependence of the transport coefficient (as a result of a low dye concentration, low temperature, or energetic disorder) cannot be ignored when we model processes in which transport competes with other events [such as, exciton disassociation, (non)radiative decay, and annihilation]. In the following, we present our results for the effective annihilation rate coefficient, obtained using the procedure illustrated in Fig. 1.

The decay of the triplet concentration, normalized to the initial concentration, is shown in Fig. 5 for a range of parameters, from which we can calculate k'_{TT} using Eqs. (8) and (9). Note that since the PL intensity is proportional to $\rho(t)$, Fig. 5 in fact illustrates the normalized PL intensity of the system. As observed in the figure, for a weak disorder or a large Förster radius, the decay clearly shows a nonexponential behavior, implying that the kinetics of the PL decay is mainly determined by the annihilation process in these cases. Also, since, according to Fig. 4, a high dye concentration results in a considerably larger diffusion coefficient, the concentration shows a prompt decay at the initial times in this situation; see the dashed-dotted curves in the plots. However, for the strong disorder [Figs. 5(c) and 5(d)] the decay slows down after the initial drop due to a small diffusion coefficient that prevents the triplets from diffusing toward each others efficiently. However, to go beyond this qualitative description and reveal the relative role of the direct and diffusion-assisted annihilation in the total annihilation rate, let us discuss the dependence of the effective rate coefficient on the various parameters.

Figure 6 shows the concentration dependence of the rate coefficient k'_{TT} for three different Förster radii, and $\sigma = 0.025$ (dashed curves) and 0.065 eV (solid curves). As seen in the figure, the effect of the energetic disorder on k'_{TT} is minimal at low concentrations, but increases as the dye concentration increases. To explain this, we note that at low concentrations, regardless of the strength of the disorder, the diffusion coefficient is small because of a large average distance between the dye molecules. Therefore, a change in the amount of disorder does not cause a significant change in the diffusion coefficient. Consequently, k'_{TT} is almost independent of σ at low N. In this regime of concentration, direct long-range Förster mechanism is the only relevant factor in determining k'_{TT}. Here it should be noted that because of the molecular aggregation in the real host-guest systems, the distance between the dye molecules at some points of the system may be different from the average value $\ell = 1/N^{\frac{1}{3}}$. In fact, as experimentally observed in real systems, the rate of the TTA may increase due to the aggregate formation, especially at high dye concentrations [7,26,62]. To model this inhomogeneous distribution of the dye molecules in a system, one needs to use network simulations in which elaborate numerical techniques can be applied to implement desired distance distribution in the simulations [63].

To separate the contribution of the diffusion process in the annihilation rate coefficient from that of the direct Förster transfer, we rewrite Eq. (4) as a sum of two terms, as

$$k_{TT}(t) = k^{\infty}_{TT} + k^{0}_{TT}, \tag{18}$$

with

$$k^{\infty}_{TT} = 4\pi \mathtt{A} \left(\frac{D^3}{\tau_F}\right)^{\frac{1}{4}} \sqrt{R_F^3}, \tag{19}$$

and

$$k^{0}_{TT} = 4\pi \mathtt{A}^2 \sqrt{\frac{1}{\tau_F \pi t}} R_F^3. \tag{20}$$

As inferred from these equations, for $D \to 0$, the rate coefficient becomes independent of the diffusion coefficient and is almost given by k^0_{TT}. This implies that, at low concentrations, the effective rate coefficient is independent of D (and σ, therefore) and is mainly determined by R_F, as seen in Fig. 6. At higher concentrations, however, the contribution of k^{∞}_{TT} to

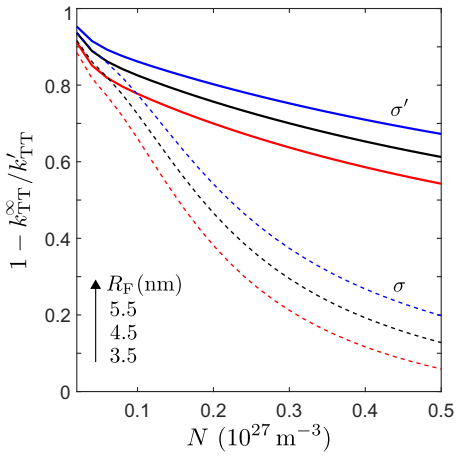

FIG. 7. Error in using Eq. (19) to estimate the annihilation rate coefficient. All the parameters are the same as in Fig. 6: $\sigma = 0.025$ and $\sigma' = 0.065$ eV, $T = 300$ K, $\alpha = 0.35$ nm, $\nu_0 = 5.5 \times 10^{11}$ s^{-1}, $\rho_0 = 10^{24}$ m^{-3}, and $\tau = 1\ \mu$s. To calculate k^{∞}_{TT}, for each data point, the value of the corresponding diffusion coefficient at time $t = \tau$ has been used in Eq. (19).

the total rate increases because as we saw in Figs. 3 and 4, the diffusion coefficient is an increasing function of N. In addition, since a lower disorder leads to a higher diffusion rate at high concentrations, the curves of low and high disorder separate from each other in this regime.

To further assess the effect of the diffusion on the annihilation process, let us compare the diffusion-assisted rate k^{∞}_{TT} to the effective rate coefficient k'_{TT}. Figure 7 illustrates the relative error $|k'_{TT} - k^{\infty}_{TT}|/k'_{TT}$ as a function of the dye concentration, for the same parameters used in Fig. 6. [Since D is time dependent, we have estimated D in Eq. (19) with $D_{t=\tau}$.] At low concentrations, for both strong and weak disorders, the diffusion has almost no effect on the annihilation process, since as seen in the figure the error is $\sim$100%. By increasing the concentration, the error decreases so that it can be concluded that for the case of the low energetic disorder (dashed curves in the figure), the annihilation process occurs mainly after some intermediate diffusive motion. For high energetic disorder, however, as can be inferred from the figure (solid curves), even at high concentrations more than $\sim$50% of the excitons annihilate via a direct long-range Förster transfer without any intermediate transport step. Also, we note that since the rates k^{∞}_{TT} and k^{0}_{TT} show different dependence on the Förster radius (as $R_F^{3/2}$ and R_F^3, respectively), with increasing the Förster radius the error also increases. In fact, a higher Förster radius enhances the probability of the direct annihilation process, resulting in a greater deviation from the rate k^{∞}_{TT}. In the following, we address the dependence of the effective rate coefficient on the Förster radius in more detail.

Figure 8 shows the effective rate k'_{TT} as a function of the Förster radius for two different strengths of the disorder. In addition to the results obtained by the model (solid curves), the scalings predicted by Eqs. (19) and (20) are also shown in the figure (dashed-dotted and dashed lines). As a general feature, it can be seen that none of these two limiting behaviors can describe the results over the whole concentration and Förster radius range shown in the figure. This result

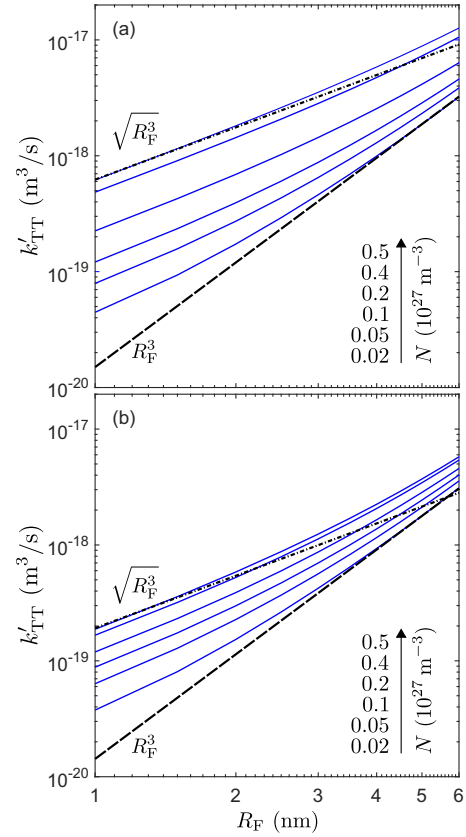

FIG. 8. The dependence of the effective rate coefficient on the Förster radius for (a) $\sigma = 0.025$ eV, and (b) $\sigma = 0.065$ eV. Other parameters are as in Figs. 6 and 7: $T = 300$ K, $\alpha = 0.35$ nm, $\nu_0 = 5.5 \times 10^{11}$ s^{-1}, $\rho_0 = 10^{24}$ m^{-3}, and $\tau = 1\ \mu$s. Dashed-dotted and dashed lines show the scaling behaviors predicted by Eq. (19) and Eq. (20), respectively.

implies that, because of the competition between the direct and diffusion-assisted annihilation, one cannot neglect either of these two mechanisms in the annihilation process. Now, let us first consider the results for the high dye concentrations. For the weak energetic disorder, the rate k'_{TT} can well be explained by the diffusion term, leading to $k'_{TT} \propto k^{\infty}_{TT} \propto R_F^{3/2}$; see Fig. 8(a). However, this does not hold for the strong disorder where the diffusion coefficient is limited because of the disorder. Therefore, by increasing the Förster radius the direct annihilation starts to have a contribution in the total annihilation rate that leads to a higher increase in k'_{TT} than that expected by the scaling $R_F^{3/2}$, as can be seen in Fig. 8(b). This is in agreement with the results of Coehoorn *et al.* who studied the triplet-polaron quenching via the Förster mechanism using the kMC simulation [64]. It must be noted that if the transport of the excitons itself occurred via the Förster mechanism with the same Förster radius as the annihilation step, one would have $k^{\infty}_{TT} \propto R_F^6$ (because for the transport via the Förster mechanism in a system with weak disorder $D \propto R_F^6$). Also, as discussed in Ref. [64], in the steady-state in which loss of the excitons is compensated by an external source, for high diffusion coefficients one observes a scaling as R_F^6 for the effective rate coefficient. Finally, if we consider the low dye concentrations in Figs. 8(a) and 8(b), it is seen that both

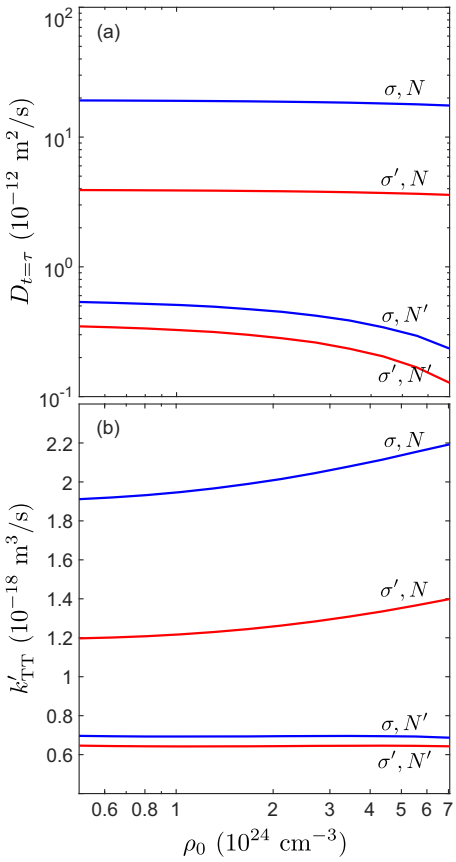

FIG. 9. (a) Dependence of the diffusion coefficient (at time $t = \tau$) on ρ_0. (b) Effect of the initial concentration of excitons, ρ_0, on the effective rate coefficient for a system with $R_F = 3.5$ nm. The parameters indicated in the figure are $\sigma = 0.025$ eV, $\sigma' = 0.065$ eV, $N = 2 \times 10^{26}$ m^{-3}, and $N' = 2 \times 10^{25}$ m^{-3}. Other parameters are the same as the previous figures: $T = 300$ K, $\alpha = 0.35$ nm, $\nu_0 = 5.5 \times 10^{11}$ s^{-1}, and $\tau = 1\,\mu$s.

the weak and strong energetic disorders lead to a similar result for the effective annihilation rate. This is because in this situation, as pointed out before, the diffusion coefficient is mainly influenced by the large distance between the dye molecules and the effect of the disorder becomes negligible.

The initial density of the excitons, ρ_0, can readily be changed in the experiment and, therefore, has been widely used to infer the mechanism of annihilation taking place in the system [13–15,28]. At first sight, it is not expected that the rate k'_{TT} will be ρ_0 dependent. This would be because, as inferred from Eq. (1), the effect of exciton concentration, ρ^2, is separated from the annihilation rate, $k_{TT}(t)$. However, it should be noted that k'_{TT} which is defined by Eq. (1) is an effective rate and, therefore, a fast decay caused by a high exciton concentration can show itself as an apparent ρ_0-dependent effective rate. In addition, the diffusion coefficient can itself show a dependence on the exciton concentration which, according to Eq. (19), results in a ρ_0-dependent annihilation rate. So, let us first discuss how the diffusion coefficient changes with the concentration of the excitons. Figure 9(a) shows our results for two dye concentrations and two different energetic disorder. As observed in the figure, for the case of the dye concentration of N, the diffusion coefficient remains almost constant over the whole range of ρ_0. For N', however, independent of the strength of the disorder, the diffusion coefficient decreases by increasing ρ_0. This is because as the concentration of the excitons approaches the dye concentration, the average number of unoccupied dyes in the vicinity of each exciton diminishes, leading gradually to a frozen state in which excitons cannot find any sites to hop to [65,66]. Note that we have assumed here that there is no spatial gradient in the exciton concentration, which can be established when the system is illuminated by a weakly absorbed light. The drop of the diffusivity at high occupancy is a general effect, which is known from the charge transport in the disordered semiconductors [45,67].

Figure 9(b) shows the dependence of k'_{TT} on ρ_0. As expected, for both the high ($N = 2 \times 10^{26}$ m^{-3}) and low ($N' = 2 \times 10^{25}$ m^{-3}) dye concentrations, the weaker disorder leads to a higher k'_{TT}, which is because of the difference in the diffusion coefficient for the weak and strong disorder cases, as we saw in Fig. 9(a). Although in the case of N' the diffusion coefficient decreases with ρ_0, it is seen in Fig. 9(b) that the effective rate coefficient is nearly constant over the range of ρ_0 presented in the figure. To explain this, we note that as observed before in Fig. 8, at low concentrations, and for $R_F \gtrsim 3$ nm, the main contribution to the annihilation process is via the direct long-range Förster and the influence of diffusion on the total rate is small. Consequently, the rate k'_{TT} becomes independent of ρ_0. In contrast, for the higher concentration of N, k'_{TT} is enhanced by increasing ρ_0. Comparing this with the results for N', we conclude that it is an effect that is originated from the higher diffusion coefficient for the case of N. (As we have shown in Supplemental Material [46], for a larger Förster radius, for example, 5 nm, k'_{TT} increases by ρ_0 even for a low dye concentration. This implies that in addition to the diffusion coefficient, a large Förster radius can also result in a ρ_0-dependent effective rate.)

Finally, we provide a direct comparison between the model presented in this work with the experimental results for a host-guest system with bis[2-(2-pyridinyl-N)phenyl-C](acetylacetonato)-iridium(III) [Ir(ppy)$_2$(acac)] as the dye molecule in a matrix of tris(4-carbazoyl-9-ylphenyl)amine (TCTA) with $\rho_0 = 10^{24}$ m^{-3}, recently reported in Ref. [28]. Figure 10 shows the effective rate coefficient as a function of the average distance between the dye molecules, that is, $1/N^{\frac{1}{3}}$. A good fit to the experimental results has been also obtained in Ref. [28] from the kMC simulation with $\alpha = 0.35$ nm, $\sigma = 0.05$ eV, $\nu_0 = 4.2 \times 10^{11}$ s^{-1}, $\tau = 1.36\,\mu$s, and $R_F = 3.5$ nm. Here, for the localization radius and the triplet lifetime we have used the same values of Ref. [28], but with a slightly different values for the width of the disorder (0.045 eV), Förster radius (3.4 nm) and attempt-to-jump frequency (8.0×10^{11} s^{-1}) we have found an excellent fit to the experimental results, as seen in Fig. 10. Considering the results in Figs. 6 and 8, we can conclude that both the direct and diffusion-assisted pathways contribute to the annihilation rate. However, the rate k'_{TT} in Fig. 10 seems to saturate at high average distances ($1/N^{\frac{1}{3}} \gtrsim 2.7$), which highlights the role of the diffusion process before reaching this regime. Also, a comparison with Fig. 2 reveals that at least part of the annihilation process occurs in the nonequilibrium conditions in which the diffusion coefficient decrease with time.

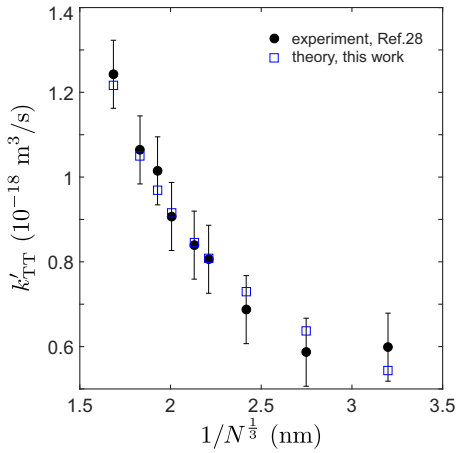

FIG. 10. Experimental (filled circles with the vertical error bar) effective rate coefficient as a function of the average distance between dye molecules for TCTA:Ir(ppy)$_2$(acac) host-guest system; from Ref. [28]. Squares show the theoretical results obtained in this work using $T = 300$ K, $\alpha = 0.35$ nm, $\sigma = 0.045$ eV, $\nu_0 = 8.0 \times 10^{11}$ s^{-1}, $\rho_0 = 10^{24}$ m^{-3}, $\tau = 1.36\,\mu$s, and $R_{\rm F} = 3.4$ nm.

IV. CONCLUSION

In this work, we have studied the effect of the energetic disorder on the triplet-triplet annihilation process in organic semiconductors. To this end, the concept of transport energy has been used to calculate the diffusion coefficient of the triplet excitons, which moves according to the Miller-Abrahams model between the dye molecules; the annihilation process, however, takes place through the Förster mechanism. An important feature arising from the energetic disorder is that, in addition to a substantial decrease in the diffusivity, the diffusion coefficient can show a time dependency during the triplet intrinsic lifetime. This implies that the annihilation of the triplets occurs in the nonequilibrium regime. Therefore, the equilibrium values for the diffusion coefficient deduced from the conventional models cannot be used in the annihilation rate coefficient. As we discussed in Sec. I, the role of diffusion on the annihilation process in organic host-guest systems has been under debate in different researches. Our results highlight the effect of diffusion on the TTA rate under certain conditions. The brief discussion presented in the previous section about Fig. 10 summarizes our conclusions that except the case of very low dye concentrations, both the direct Förster transfer and the diffusion process (accompanied by a Förster transfer) contribute to the effective annihilation rate. The fit in Fig. 10 shows that the method presented in this work can be used to model the annihilation process and also to examine the time-resolved phosphorescence and delayed fluorescence experiments in the disordered semiconductors. It should also be noted that the recipe suggested here, Fig. 1, can also straightforwardly be extended to the case of the singlet-singlet annihilation, as will be presented in future work.

[1] A. Köhler and H. Bässler, *Electronic Processes in Organic Semiconductors: An Introduction* (John Wiley & Sons, New York, 2015).
[2] O. Ostroverkhova, Organic optoelectronic materials: mechanisms and applications, Chem. Rev. **116**, 13279 (2016).
[3] O. V. Mikhnenko, P. W. Blom, and T.-Q. Nguyen, Exciton diffusion in organic semiconductors, Energ. Environ. Sci. **8**, 1867 (2015).
[4] J. Zhou, Q. Liu, W. Feng, Y. Sun, and F. Li, Upconversion luminescent materials: advances and applications, Chem. Rev. **115**, 395 (2014).
[5] P. Mahato, A. Monguzzi, N. Yanai, T. Yamada, and N. Kimizuka, Fast and long-range triplet exciton diffusion in metal–organic frameworks for photon upconversion at ultralow excitation power, Nature Mater. **14**, 924 (2015).
[6] M. A. Baldo, C. Adachi, and S. R. Forrest, Transient analysis of organic electrophosphorescence. II. transient analysis of triplet-triplet annihilation, Phys. Rev. B **62**, 10967 (2000).
[7] C. Murawski, K. Leo, and M. C. Gather, Efficiency roll-off in organic light-emitting diodes, Adv. Mater. **25**, 6801 (2013).
[8] N. C. Giebink, Y. Sun, and S. Forrest, Transient analysis of triplet exciton dynamics in amorphous organic semiconductor thin films, Org. Electron. **7**, 375 (2006).
[9] S. T. Hoffmann, J.-M. Koenen, U. Scherf, I. Bauer, P. Strohriegl, H. Bässler, and A. Köhler, Triplet–triplet annihilation in a series of poly (p-phenylene) derivatives, J. Phys. Chem. B **115**, 8417 (2011).
[10] Y. Zhang and S. R. Forrest, Triplet diffusion leads to triplet–triplet annihilation in organic phosphorescent emitters, Chem. Phys. Lett. **590**, 106 (2013).
[11] H. Van Eersel, P. Bobbert, and R. Coehoorn, Kinetic monte carlo study of triplet-triplet annihilation in organic phosphorescent emitters, J. Appl. Phys. **117**, 115502 (2015).
[12] F. Fennel and S. Lochbrunner, Exciton-exciton annihilation in a disordered molecular system by direct and multistep förster transfer, Phys. Rev. B **92**, 140301(R) (2015).
[13] E. Engel, K. Leo, and M. Hoffmann, Ultrafast relaxation and exciton–exciton annihilation in ptcda thin films at high excitation densities, Chem. Phys. **325**, 170 (2006).
[14] W. Staroske, M. Pfeiffer, K. Leo, and M. Hoffmann, Single-Step Triplet-Triplet Annihilation: An Intrinsic Limit for the High Brightness Efficiency of Phosphorescent Organic Light Emitting Diodes, Phys. Rev. Lett. **98**, 197402 (2007).
[15] L. Zhang, H. van Eersel, P. Bobbert, and R. Coehoorn, Clarifying the mechanism of triplet–triplet annihilation in phosphorescent organic host–guest systems: A combined experimental and simulation study, Chem. Phys. Lett. **652**, 142 (2016).
[16] R. Coehoorn, P. A. Bobbert, and H. van Eersel, Effect of exciton diffusion on the triplet-triplet annihilation rate in organic semiconductor host-guest systems, Phys. Rev. B **99**, 024201 (2019).
[17] V. May and O. Kühn, *Charge and Energy Transfer Dynamics in Molecular Systems* (John Wiley & Sons, New York, 2008).
[18] A. Köhler and H. Bässler, What controls triplet exciton transfer in organic semiconductors? J. Mater. Chem. **21**, 4003 (2011).

[19] S. Baranovski, *Charge Transport in Disordered Solids with Applications in Electronics*, Vol. 17 (John Wiley & Sons, New York, 2006).

[20] S. Baranovskii, Theoretical description of charge transport in disordered organic semiconductors, Phys. Stat. Sol. B **251**, 487 (2014).

[21] M. Scheidler, B. Cleve, H. Bässler, and P. Thomas, Monte carlo simulation of bimolecular exciton annihilation in an energetically random hopping system, Chem. Phys. Lett. **225**, 431 (1994).

[22] M. Ansari-Rad and S. Athanasopoulos, Theoretical study of equilibrium and nonequilibrium exciton dynamics in disordered semiconductors, Phys. Rev. B **98**, 085204 (2018).

[23] B. Valeur and M. N. Berberan-Santos, *Molecular Fluorescence: Principles and Applications* (John Wiley & Sons, New York, 2012).

[24] T.-S. Ahn, N. Wright, and C. J. Bardeen, The effects of orientational and energetic disorder on forster energy migration along a one-dimensional lattice, Chem. Phys. Lett. **446**, 43 (2007).

[25] C. Madigan and V. Bulović, Modeling of Exciton Diffusion in Amorphous Organic Thin Films, Phys. Rev. Lett. **96**, 046404 (2006).

[26] Y. Kawamura, J. Brooks, J. J. Brown, H. Sasabe, and C. Adachi, Intermolecular Interaction and a Concentration-Quenching Mechanism of Phosphorescent Ir (iii) Complexes in a Solid Film, Phys. Rev. Lett. **96**, 017404 (2006).

[27] R. R. Lunt, N. C. Giebink, A. A. Belak, J. B. Benziger, and S. R. Forrest, Exciton diffusion lengths of organic semiconductor thin films measured by spectrally resolved photoluminescence quenching, J. Appl. Phys. **105**, 053711 (2009).

[28] A. Ligthart, X. de Vries, L. Zhang, M. C. Pols, P. A. Bobbert, H. van Eersel, and R. Coehoorn, Effect of triplet confinement on triplet–triplet annihilation in organic phosphorescent host–guest systems, Adv. Funct. Mater. **28**, 1804618 (2018).

[29] J. Saxton, Anomalous diffusion due to obstacles: A monte carlo study, Biophys. J. **66**, 394 (1994).

[30] U. Gösele, M. Hauser, U. Klein, and R. Frey, Diffusion and long-range energy transfer, Chem. Phys. Lett. **34**, 519 (1975).

[31] P. R. Butler and M. J. Pilling, The breakdown of förster kinetics in low viscosity liquids. an approximate analytical form for the time-dependent rate constant, Chem. Phys. **41**, 239 (1979).

[32] S. A. Rice, *Diffusion-Limited Reactions*, Vol. 25 (Elsevier, Amsterdam, 1985).

[33] B. Movaghar, M. Grünewald, B. Ries, H. Bässler, and D. Würtz, Diffusion and relaxation of energy in disordered organic and inorganic materials, Phys. Rev. B **33**, 5545 (1986).

[34] S. T. Hoffmann, E. Scheler, J.-M. Koenen, M. Forster, U. Scherf, P. Strohriegl, H. Bässler, and A. Köhler, Triplet energy transfer in conjugated polymers. iii. an experimental assessment regarding the influence of disorder on polaronic transport, Phys. Rev. B **81**, 165208 (2010).

[35] X. Liu, Y. Zhang, and S. R. Forrest, Temperature dependence of the exciton dynamics in DCM2: Alq_3, Phys. Rev. B **90**, 085201 (2014).

[36] S. T. Hoffmann, S. Athanasopoulos, D. Beljonne, H. Bässler, and A. Köhler, How do triplets and charges move in disordered organic semiconductors? A Monte Carlo study comprising the equilibrium and nonequilibrium regime, J. Phys. Chem. C **116**, 16371 (2012).

[37] R. Kersting, U. Lemmer, R. F. Mahrt, K. Leo, H. Kurz, H. Bässler, and E. O. Göbel, Femtosecond Energy Relaxation in π-Conjugated Polymers, Phys. Rev. Lett. **70**, 3820 (1993).

[38] S. D. Baranovskii, R. Eichmann, and P. Thomas, Temperature-dependent exciton luminescence in quantum wells by computer simulation, Phys. Rev. B **58**, 13081 (1998).

[39] O. Mikhnenko, F. Cordella, A. Sieval, J. Hummelen, P. Blom, and M. Loi, Temperature dependence of exciton diffusion in conjugated polymers, J. Phys. Chem. B **112**, 11601 (2008).

[40] S. T. Hoffmann, H. Bässler, J.-M. Koenen, M. Forster, U. Scherf, E. Scheler, P. Strohriegl, and A. Köhler, Spectral diffusion in poly (para-phenylene)-type polymers with different energetic disorder, Phys. Rev. B **81**, 115103 (2010).

[41] G. M. Akselrod, F. Prins, L. V. Poulikakos, E. M. Lee, M. C. Weidman, A. J. Mork, A. P. Willard, V. Bulović, and W. A. Tisdale, Subdiffusive exciton transport in quantum dot solids, Nano Lett. **14**, 3556 (2014).

[42] G. M. Akselrod, P. B. Deotare, N. J. Thompson, J. Lee, W. A. Tisdale, M. A. Baldo, V. M. Menon, and V. Bulović, Visualization of exciton transport in ordered and disordered molecular solids, Nature Commun. **5**, 3646 (2014).

[43] S. Athanasopoulos, S. T. Hoffmann, H. Bässler, A. Köhler, and D. Beljonne, To hop or not to hop? Understanding the temperature dependence of spectral diffusion in organic semiconductors, J. Phys. Chem. Lett. **4**, 1694 (2013).

[44] D. Monroe, Hopping in Exponential Band Tails, Phys. Rev. Lett. **54**, 146 (1985).

[45] J. O. Oelerich, D. Huemmer, and S. D. Baranovskii, How to Find Out the Density of States in Disordered Organic Semiconductors, Phys. Rev. Lett. **108**, 226403 (2012).

[46] See Supplemental Material at http://link.aps.org/supplemental/10.1103/PhysRevB.101.094204 for the derivation of the transport energy and diffusion coefficient, and dependence of the effective rate coefficient on the initial concentration of the excitons.

[47] S. V. Novikov, D. H. Dunlap, V. M. Kenkre, P. E. Parris, and A. V. Vannikov, Essential Role of Correlations in Governing Charge Transport in Disordered Organic Materials, Phys. Rev. Lett. **81**, 4472 (1998).

[48] J. Cottaar, R. Coehoorn, and P. A. Bobbert, Scaling theory for percolative charge transport in molecular semiconductors: Correlated versus uncorrelated energetic disorder, Phys. Rev. B **85**, 245205 (2012).

[49] S. D. Baranovskii, H. Cordes, F. Hensel, and G. Leising, Charge-carrier transport in disordered organic solids, Phys. Rev. B **62**, 7934 (2000).

[50] J. Bisquert, Interpretation of electron diffusion coefficient in organic and inorganic semiconductors with broad distributions of states, Phys. Chem. Chem. Phys. **10**, 3175 (2008).

[51] T. Tiedje and A. Rose, A physical interpretation of dispersive transport in disordered semiconductors, Solid State Commun. **37**, 49 (1981).

[52] B. I. Shklovskii and A. L. Efros, *Electronic Properties of Doped Semiconductors*, Vol. 45 (Springer, Berlin, 1984).

[53] H. Bässler, Charge transport in disordered organic photoconductors a monte carlo simulation study, Phys. Stat. Sol. B **175**, 15 (1993).

[54] D. Ben-Avraham and S. Havlin, *Diffusion and Reactions in Fractals and Disordered Systems* (Cambridge University Press, Cambridge, 2000).

[55] K. Benkstein, N. Kopidakis, J. van de Lagemaat, and A. Frank, Influence of the percolation network geometry on electron transport in dye-sensitized titanium dioxide solar cells, J. Phys. Chem. B **107**, 7759 (2003).

[56] M. Ansari-Rad, Y. Abdi, and E. Arzi, Monte carlo random walk simulation of electron transport in dye-sensitized nanocrystalline solar cells: Influence of morphology and trap distribution, J. Phys. Chem. C **116**, 3212 (2012).

[57] D. Hertel, H. Bässler, R. Guentner, and U. Scherf, Triplet-triplet annihilation in a poly (fluorene)-derivative, J. Chem. Phys. **115**, 10007 (2001).

[58] C. Rothe, S. M. King, F. Dias, and A. P. Monkman, Triplet exciton state and related phenomena in the β-phase of poly (9, 9-dioctyl) fluorene, Phys. Rev. B **70**, 195213 (2004).

[59] V. Jankus, C.-J. Chiang, F. Dias, and A. P. Monkman, Deep blue exciplex organic light-emitting diodes with enhanced efficiency; p-type or e-type triplet conversion to singlet excitons? Adv. Mater. **25**, 1455 (2013).

[60] J. Oelerich, F. Jansson, A. Nenashev, F. Gebhard, and S. Baranovskii, Energy position of the transport path in disordered organic semiconductors, J. Phys.: Condens. Matter **26**, 255801 (2014).

[61] See Supplemental Material of Ref. [16] at http://link.aps.org/supplemental/10.1103/PhysRevB.101.094204.

[62] S. Reineke, G. Schwartz, K. Walzer, M. Falke, and K. Leo, Highly phosphorescent organic mixed films: The effect of aggregation on triplet-triplet annihilation, Appl. Phys. Lett. **94**, 116305 (2009).

[63] B. Baumeier, O. Stenzel, C. Poelking, D. Andrienko, and V. Schmidt, Stochastic modeling of molecular charge transport networks, Phys. Rev. B **86**, 184202 (2012).

[64] R. Coehoorn, P. A. Bobbert, and H. van Eersel, Förster-type triplet-polaron quenching in disordered organic semiconductors, Phys. Rev. B **96**, 184203 (2017).

[65] T. Ala-Nissila, R. Ferrando, and S. Ying, Collective and single particle diffusion on surfaces, Adv. Phys. **51**, 949 (2002).

[66] M. Ansari-Rad, J. A. Anta, and J. Bisquert, Interpretation of diffusion and recombination in nanostructured and energy-disordered materials by stochastic quasiequilibrium simulation, J. Phys. Chem. C **117**, 16275 (2013).

[67] R. Coehoorn, W. F. Pasveer, P. A. Bobbert, and M. A. J. Michels, Charge-carrier concentration dependence of the hopping mobility in organic materials with gaussian disorder, Phys. Rev. B **72**, 155206 (2005).